coatings

MDPI

Article

Multi-Objective Optimization of Surface Integrity in the Grind-Hardening Process

Chunyan Wang *, Guicheng Wang, Chungen Shen and Xinyu Dai

School of Mechanical Engineering, Jiangsu University, Zhenjiang 212013, China; wgch@ujs.edu.cn (G.W.); chungens@163.com (C.S.)
* Correspondence: wangchunyan@ujs.edu.cn

Abstract: Grind-hardening machining is a new integrated manufacturing technology that integrates the theory of material surface quenching and grinding machining. The surface integrity of grind-hardening directly affects the performance and reliability of the parts. Improving the grind-hardening quality has always been the focus and difficulty in this field. Based on the surface integrity theory and the characteristics of the grind-hardening process, this paper proposed four optimization criteria for grinding parameters according to the engineering application requirements of materials. Using the expectation function, the burr cross-sectional area, depth of the effective hardened layer, and surface roughness were comprehensively analyzed under each optimization criterion to obtain an optimal combination of grinding parameters. The results revealed a significant inconsistency in the optimized grinding parameters under each optimization criterion. When considering the depth of the effective hardened layer as the primary optimization parameter and ignoring the surface roughness and burr cross-sectional area, the highest overall desirability was 0.926395. In practical application, the optimization criteria should be reasonably selected according to the actual engineering requirements.

Keywords: surface integrity; grind-hardening; burr cross-sectional area; depth of the effective hardened layer; surface roughness

Citation: Wang, C.; Wang, G.; Shen, C.; Dai, X. Multi-Objective Optimization of Surface Integrity in the Grind-Hardening Process. *Coatings* **2024**, *14*, 910. https://doi.org/10.3390/coatings14070910

Academic Editor: Alexander Tolstoguzov

Received: 2 June 2024
Revised: 21 June 2024
Accepted: 8 July 2024
Published: 20 July 2024

1. Research Background

The grind-hardening process was proposed by two German academics, Brinksmeier E. and Brockhoff T., in 1994 [1]. Grinding hardening is a short time austenization of the surface layer structure to achieve martensitic phase transformation, followed by self-quenching. The hardness was significantly improved, the residual stress of the surface layer was mainly manifested as compressive stress, and the wear resistance was significantly improved. Grind-hardening is not only an alternative to induction hardening and laser hardening but also an alternative to traditional surface strengthening. It integrates the heat treatment process of surface quenching into the production line and processing process of grinding, improves the processing efficiency and reduces the cost, and is a green composite processing technology [2]. Liu Judong et al. studied the formation mechanism and influencing factors of grind-hardened layers of steel 65Mn, steel 40Cr, and steel AISI 1066 through grind-hardening tests. Martensitic phase transformation took place on all surfaces, and a certain depth of hardened layer was produced. The results showed that the grind-hardened layer consists of a complete hardening zone and a transition zone. The fully hardened layer formed a uniform fine martensite [3–5]. The finite element analysis combined with experiments showed that the grind-hardening process is suitable for non-plane. By reducing the workpiece feed speed, the heating time could be increased, so that the heat could penetrate deeper and expand more widely in the workpiece, and the hardening layer was thicker. The cylindrical grind-hardening process could be optimized by changing the grinding dosage [6–8].

2. Current Status of Research on Surface Integrity in Grinding Operations

Surface integrity is an important factor in evaluating the quality of machined surfaces and has been a research hotspot over the years. Previous studies have shown that within the constraints of other conditions, grinding parameters have a significant impact on the integrity of the grinding surface, and the surface quality can be improved by varying the machining parameters [9,10].

Liu et al. used ceramic bond CBN grinding wheels for high-speed grinding of non-circular equidistant profiles with an X-C axis linkage. The effects of grinding parameters on grinding temperature, surface roughness, and residual stress were analyzed. The results showed that with increasing wheel speed, the grinding temperature increased, the residual stress increased, and the surface roughness decreased. As the workpiece speed increased, the grinding temperature and residual stresses decreased, and the surface roughness increased. With increasing grinding depth, the grinding temperature, residual stress, and surface roughness increased. In addition, the depth of grinding exhibited the greatest influence on residual stresses, followed by wheel speed and workpiece speed. These results indicated that grinding parameters have an important effect on grinding surface quality, and surface quality can be improved by changing the grinding parameters [9]. Xiao et al. performed grinding experiments to investigate the effects of different processing parameters on the surface integrity of GH4169. Their effects on the surface morphology, roughness, and residual stresses were also explored. The results showed that different parameters of the band grinding can significantly change surface integrity indicators such as surface morphology, roughness, and residual stress. Roughness mainly affects stress concentration. Macroscopically, a greater degree of roughness makes it easier to sprout cracks. Residual stresses inhibit crack initiation and slow crack propagation [11]. Zhao et al. used ductile iron QT700-2 as the test material to study the effects of grinding parameters on grinding force, material removal rate, grinding temperature, and surface integrity in shape adaptive grinding (SAG). The results showed that the particle size of the surfactant was the most important factor affecting the grinding force, material removal rate, and surface roughness. The influence law of the SAG process on the surface integrity of ductile iron QT700-2 was summarized, and the optimal grinding parameters were obtained [12].

Regarding the surface integrity of grind-hardened components, most of the studies analyzed it from a single or two aspects, and less research was conducted from the perspective of multi-objective optimization according to the actual engineering needs. Based on numerical simulations and experimental studies, Wang et al. analyzed the integrity of grind-hardened surfaces from a single or two aspects, and the prongs (burrs) were included in the evaluation of grind-hardening quality. The results showed that changes in grinding parameters played an important role in increasing the effective hardened layer depth and improving surface quality and edge quality [13–16]. Hong et al. studied the formation mechanism of the grind-hardened layer from the microscopic scale, discussed the quantitative relationship between the microstructure and the macroscopic hardening characteristics of the surface, and proposed a hardness prediction method for grinding surfaces based on surface microstructure distribution [17]. Zhao et al. investigated the effect of grinding parameters on the uniformity of hardened layers [18].

The surface integrity of the grind-hardening process directly affects the service performance of components and their reliability. Improving and enhancing the quality of grind-hardening has been the focus and difficulty in this field. Therefore, it is of great theoretical significance and engineering application value to systematically investigate the surface integrity in the grind-hardening process. Based on modern processing quality theory, the surface integrity of the components processed by grind-hardening can be subdivided into surface quality, surface layer quality, and edge quality according to the characteristics of grind-hardening processing. Each element consists of different characterization metrics with components of surface integrity, as shown in Figure 1. Based on the grind-hardening response surface test, this study provided a comprehensive optimization and analysis of multiple indicators affecting surface integrity according to the theory of

machining surface integrity. The optimal selection method of grinding parameters for the grind-hardening process was explored.

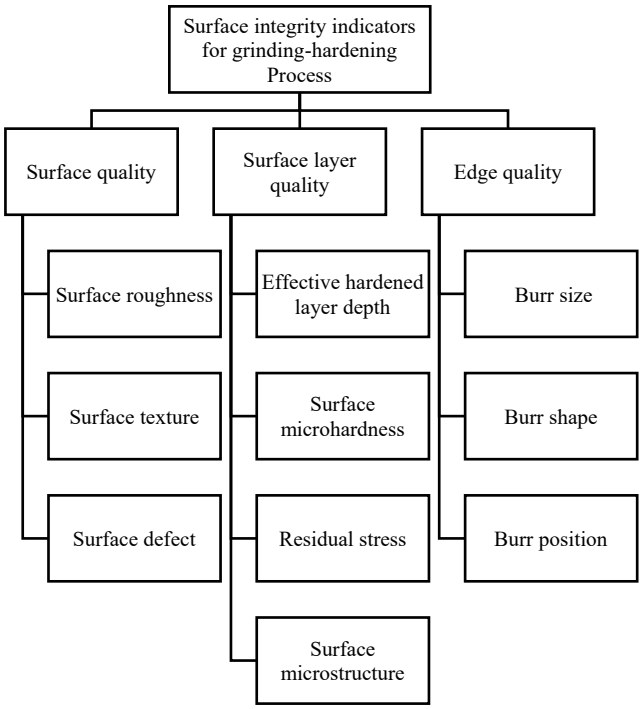

Figure 1. Elements of surface integrity.

3. Design of the Grind-Hardening Process

3.1. Test Platform Construction

Grind-hardening is a surface-hardening process achieved through the utilization of heat generated during grinding. To achieve a satisfactory depth of the hardened layer, it is imperative to optimize both the heat generation during grinding and the heat transfer to the workpiece surface. This test was carried out on a slow-feed surface CNC grinder (Model MKL7132 × 6/12, Hangzhou Machine Tool Factory, Hangzhou, China) in dry and forward grinding mode. A white corundum grinding wheel (WA60L6V, Zhengzhou Abrasives Grinding Institute Co., LTD, Zhengzhou, China) with a ceramic bond was selected. Before each group of tests, the grinding wheel was dressed with a diamond dressing pen, and the dressing parameters of the grinding wheel were shown in Table 1. The grind-hardening test bench is shown in Figure 2, and the sample piece was fixed to the grinding machine with a holder.

Table 1. Parameters of wheel dressing.

Dressing Steps	Wheel Speed (m/s)	Dressing Depth (mm)	Dressing Feed Speed (mm/s)	Dressing Times
Preliminary	25	0.02	1.5	2
Truing	25	0.01	1.5	2

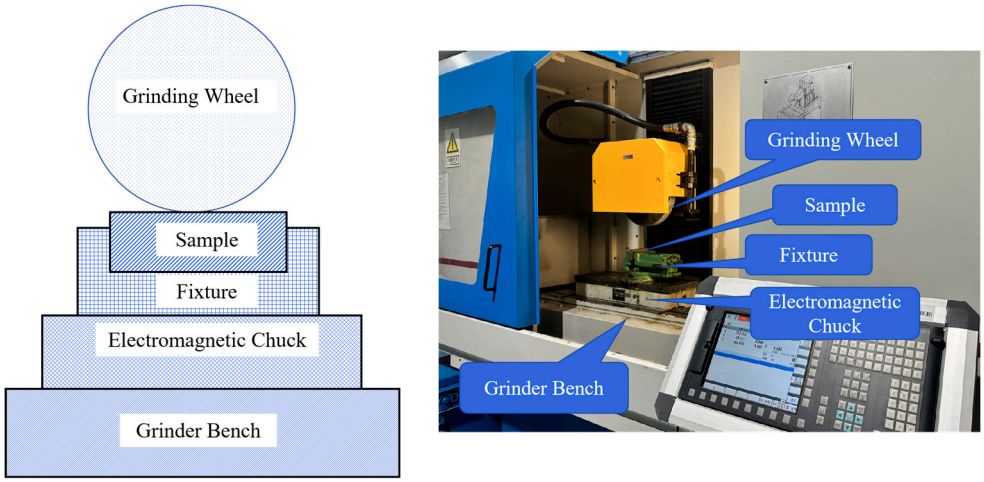

Figure 2. Grind-hardening test platform. (**a**) Connection diagram of test device (**b**) Test system of grind-hardening.

3.2. Test Material

42CrMo steel is often employed in many large machinery crankshafts, connecting rods, heavy-duty bearings, high-strength bolts, and other important components. Therefore, it is of great engineering importance to study the optimization of its surface integrity in the grind-hardening process. This alloy steel is characterized by high hardenability and structural stability. Its chemical composition is shown in Table 2, and its mechanical properties are shown in Table 3 [19]. Samples were pre-conditioned and cut into a cuboid of 60 mm × 20 mm × 25 mm. In order to avoid the geometric errors and clamping errors of the sample affecting the grinding process, the surface grinder was used to fine-grind the surface and side of the workpiece. Finally, the edge, corner, and other parts of the workpiece were polished with sandpaper.

Table 2. Chemical composition of 42CrMo steel (wt.%).

Composition	wt.%	Composition	wt.%
Cr	0.90–1.20	Mn	0.50–0.80
C	0.38–0.45	Cu/Ni	≤0.30
Mo	0.15–0.25	P	≤0.035
S	≤0.035	Si	0.17–0.37

Table 3. Mechanical behavior of 42CrMo steel.

Tensile Strength σ_b (MPa)	Yield Strength σ_s (MPa)	Hardness (HB)	Elongation δ (%)	Reduction of Area ψ (%)
≥1080	≥930	≤217	≥12	≥45

3.3. Experimental Design of the Response Surface

According to the preliminary grind-hardening process, under air-cooled conditions, when the grinding wheel speed v_s was 25–35 m/s, the workpiece feed speed v_w was 0.2–0.6 m/min, and the grinding depth a_p was 0.2–0.4 mm, the hardness of the high hardening zone of the grind-hardened layer was always between 620 and 700 HV [14]. Under these conditions, the average depth of the hardened layer was 1.9 mm and favorable hardening results could be achieved. In this test, the Box–Behnken response surface design method was adopted to set up a three-factor, three-level test with the workpiece feed rate v_w (m/min), grinding depth a_p (mm), and grinding wheel speed v_s (m/s) as three factors, in

which the 0-level parameter was the intermediate level automatically generated according to the three-factor, three-level system, and the factor coding and grinding parameter settings are shown in Table 4. The experimental design was carried out in software DESIGN EXPERT 12. After grind-hardening, the samples were cooled in air.

Table 4. Grinding parameter setting in grind-hardening test.

Grinding Parameter	Unit	Factor Coding	Parameter Setting		
			−1	0	1
The workpiece feed rate v_w	m/min	X_1	0.2	0.4	0.6
Grinding depth a_p	mm	X_2	0.2	0.3	0.4
Grinding wheel speed v_s	m/s	X_3	25	30	35
Grinding mode	One way, forward grinding, full width grinding				

3.4. Test Results

(1) Surface roughness measurement: The previous study demonstrated unevenness in the surface topography after the grind-hardening process, which could be roughly divided into the cut-in, intermediate, and cut-out zones. In the cut-in zone, the grinding texture was clearer, but there were more bonding and trace damage phenomena; the intermediate zone was flatter, with a small amount of bonding and some damage; and in the cut-out zone, the grinding texture was coarse, with more microcracks and grinding damage [16]. Therefore, this study divided the specimen into the cut-in, intermediate, and cut-out zones, and the processed surface was cleaned with a soft cloth and fine sandpaper. Five measurements were taken perpendicular to the grinding direction in each of the three zones using an optical digital microscope, as shown in Figure 3. The maximum and minimum values in each zone were removed, and the remaining values were taken as the roughness measurement results.

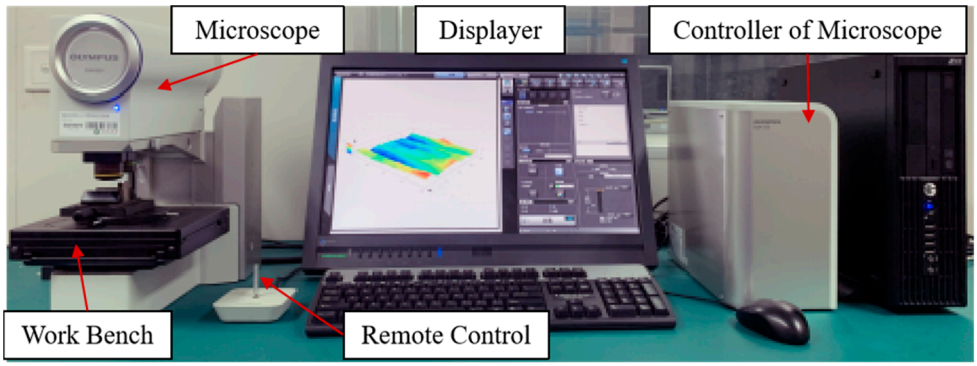

Figure 3. OLYMPUS-DSX500 Optical Microscope.

(2) Burr feature size measurement: The specimen was cut into 10 small specimens of 6 mm × 20 mm × 25 mm (length × width × height) along the length direction with an EDM cutter, and sandpaper of different grit sizes from coarse to fine was used to polish the specimen. The cross-sectional area of the burr was influenced by a combination of factors, including burr height, burr root thickness, and burr root radius. These factors reflect the size of the burr entity volume and directly impact the difficulty of burr removal. Therefore, the burr cross-sectional area serves as an indicator of the edge (burr). An optical digital microscope (OLYMPUS-DSX500, Olympus Corporation, Tokyo, Japan) was employed to measure the burr cross-sectional area S, as shown in Figure 4. The average value of the burr sizes on the left and right sides of the stabilization zone of the specimen was determined.

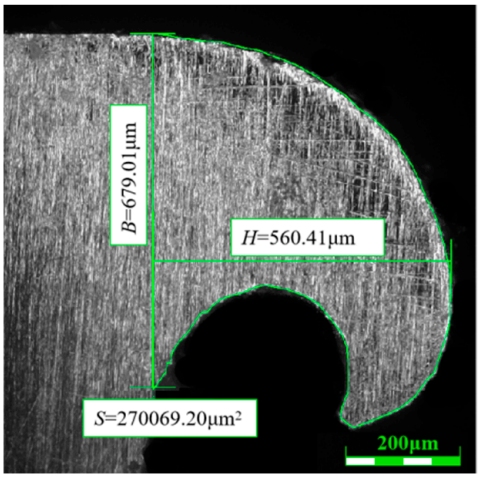

Figure 4. Diagram of burr measurement.

(3) Measurement of the effective hardened layer depth: The first and second sets of specimens were continuously tested for surface hardness and depth of the hardened layer to investigate the formation and changes in the grind-hardened surface layer. Different types of sandpaper (from coarse to fine) were used to smooth the surface, and the polishing machine was adopted to polish the surface to the mirror requirements. Microhardness was measured at 0.2 mm intervals in the depth direction of the grind-hardened layer using an HVS-1000 digital hardness tester(Shanghai Lunjie Electromechanical Instrument Co., Ltd., Shanghai, China).

When half of the microstructure of the workpiece was martensite and half was non-martensite, a "half martensite" area was formed, facilitating microscopic observation and exhibiting the most significant change in hardness. Therefore, the depth of the hardened layer can be easily determined based on the hardness in the semi-martensitic zone of steels with different carbon contents using the hardness distribution curves obtained from cross-sectional measurements of hardened steel components, as shown in Figure 5 [20]. The carbon content of 42CrMo steel was 0.38–0.45, and the hardness of "half-martensite" was about 38–45 HRC. In order to facilitate the measurement and calculation, the upper limit of 45 HRC was taken, which was about 450 HV [21]. That is, the hardness value of more than 450 HV was regarded as an effective hardened layer. The measurement schematic is shown in Figure 6, and the depth of the effective hardened layer for this specimen was 2.31 mm.

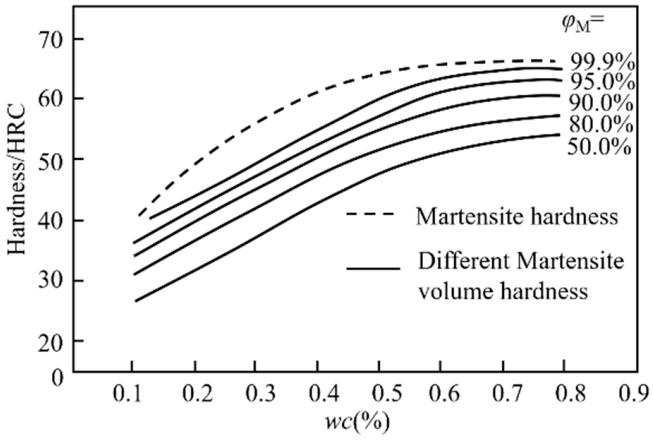

Figure 5. Relationship between semi-martensitic hardness and carbon content of steel.

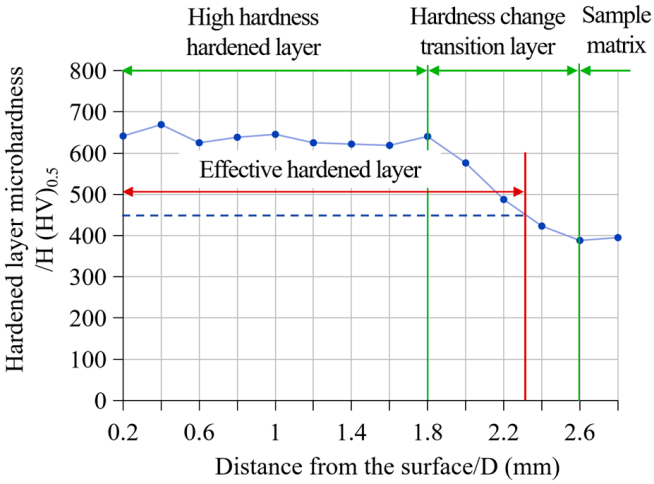

Figure 6. Measurement diagram of effective hardened layer (Sample No. 7).

The experimental design, sample numbers, and measurements of surface roughness (*Ra*, μm), burr cross-sectional area (*S*, mm^2), and depth of the effective roughness layer (*h*, mm) for all samples are summarized in Table 5.

Table 5. Test results of response surface grind-hardening tests.

No.	v_w (m/min)	a_p (mm)	v_s (m/s)	*Ra* (μm)	*h* (mm)	*S* (mm^2)
1	0.2	0.2	30	1.28	1.98	0.3661
2	0.6	0.2	30	1.85	1.16	0.2510
3	0.2	0.4	30	1.81	2.64	0.7112
4	0.6	0.4	30	2.54	1.41	0.2923
5	0.2	0.3	25	2.26	2.21	0.3957
6	0.6	0.3	25	2.3	1.27	0.1470
7	0.2	0.3	35	2.03	2.31	0.4016
8	0.6	0.3	35	2.30	1.43	0.1900
9	0.4	0.2	25	1.87	1.30	0.2408
10	0.4	0.4	25	2.39	1.69	0.4316
11	0.4	0.2	35	1.56	1.57	0.2643
12	0.4	0.4	35	2.29	1.99	0.4738
13	0.4	0.3	30	1.91	1.73	0.3434
14	0.4	0.3	30	2.06	1.75	0.3163
15	0.4	0.3	30	2.10	1.86	0.3097
16	0.4	0.3	30	1.95	1.81	0.3188
17	0.4	0.3	30	1.85	1.71	0.3388

4. Influence of Grinding Parameters on the Integrity of Grind-Hardened Surfaces

4.1. Influence of Grinding Parameter on Surface Roughness of Grind-Hardened Surfaces

It can be seen from Figure 7 that within the range of parameters, the surface roughness shows an increasing trend with the increase in both the grinding depth and the workpiece feed rate. In contrast, the surface roughness showed a trend of first decreasing and then increasing with the increase in grinding wheel speed in the range of parameters in this test.

According to the grinding mechanism, an increase in grinding depth and workpiece feed rate leads to a higher number of effective dynamic grinding edges, resulting in an elevated maximum undeformed chip thickness, increased grinding force, and heat generation. Consequently, it induces a greater degree of plastic deformation and stress on the material, ultimately leading to an increase in surface roughness (*Ra*) value. With the increase in grinding speed, the density of the grinding edge on the contact surface between the workpiece and grinding wheel increases in unit time, the maximum thickness of the undeformed chip becomes smaller, the grinding force becomes smaller, and the surface roughness shows a decreasing trend. However, the strain of grinding chips increases due

to the size effect, leading to an increase in grinding temperature, plastic deformation, and surface roughness [17].

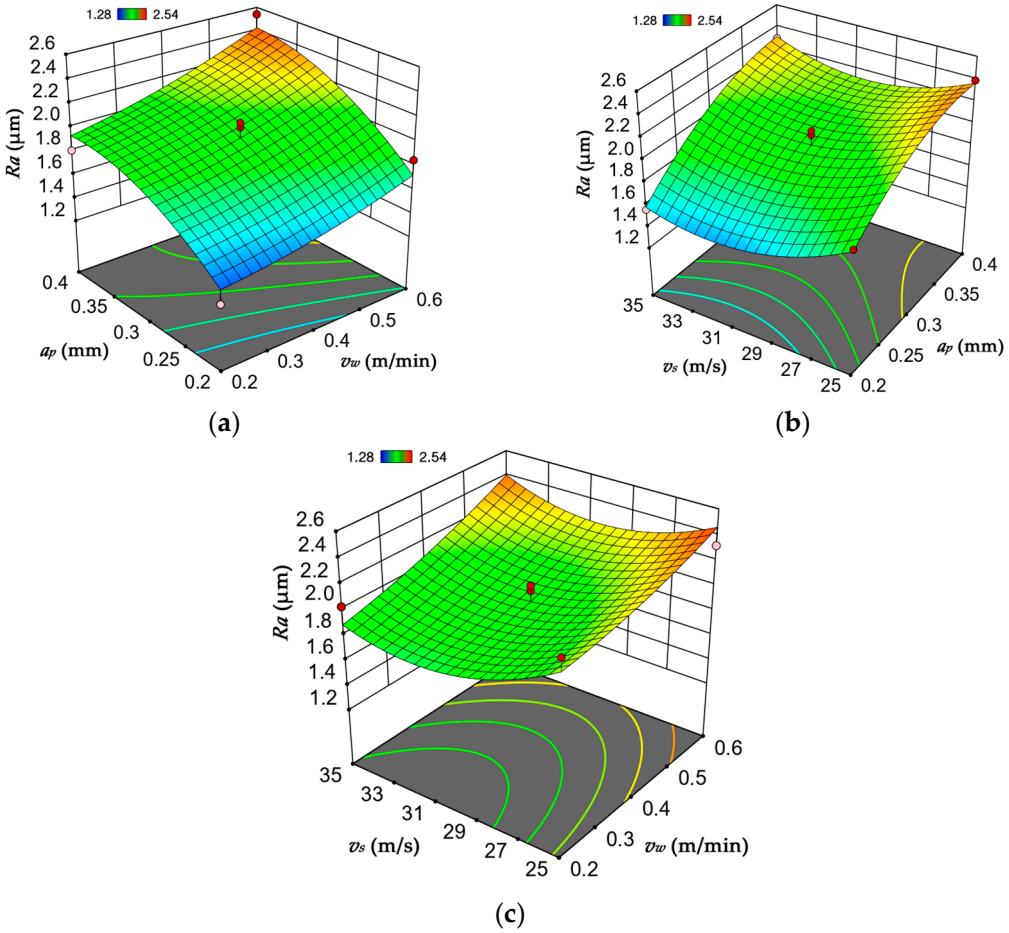

Figure 7. (**a**) Contour map of grinding depth-grinding linear velocity (v_s = 30 m/s); (**b**) contour map of grinding depth–workpiece feed rate (v_w = 0.4 m/min); (**c**) contour map of grinding linear velocity-workpiece feed velocity (a_p = 0.3 mm).

4.2. Influence of Grinding Parameter on the Depth of Hardened Layer

As can be seen from the contour map in Figure 8, under this test condition, the depth of the hardened layer increases with the decrease in workpiece feed speed and the increase in grinding depth and grinding wheel speed [22].

The depth of the grind-hardened layer was mainly influenced by the grinding temperature and thermal action time. With a decrease in the workpiece feed speed, the effective number of grinding edges per unit of time was reduced, leading to a reduction in heat flow density and grinding force. Consequently, the grinding temperature decreased; however, it still remained higher than the critical temperature for material phase transition. The thermal action time increased proportionally with the contact time between the grinding wheel and the workpiece, allowing sufficient heat transfer to occur within the inner layer. Accordingly, the depth of the hardened layer increased. As the grinding wheel speed increased, plowing and sliding abrasion intensified, with higher grinding temperature and a larger depth of the grind-hardened layer. However, the increase in the number of effective grinding edges per unit of time also led to a decrease in the maximum undeformed chip thickness of the grits and a reduction in the grinding force, resulting in a gradual increase in the depth of the hardened layer. As the grinding depth increased, the contact area between the grinding wheel and the workpiece increased, prolonging the thermal action time. Subsequently, the grinding temperature had more time to be transmitted to

the inside of the workpiece, thus increasing the depth of the hardened layer. At the same time, the number of effective grinding edges in the unit contact area increased, leading to an increase in the volume of a single abrasive grain pressed into the workpiece. Finally, the maximum undeformed chip thickness during grinding and the resultant grinding forces were increased, which also led to higher grinding temperatures and an increase in the depth of the hardened layer.

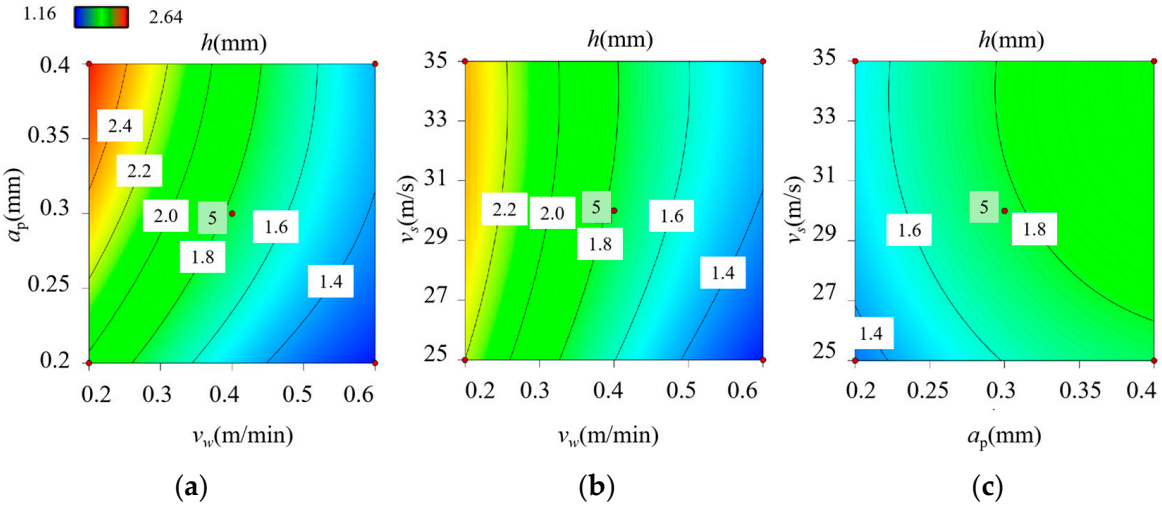

Figure 8. Contour map of the influence of grinding parameter on the depth of hardened layer (**a**) grinding depth—workpiece feed speed (v_s = 30 m/s); (**b**) grinding wheel speed—workpiece feed speed (a_p = 0.3 mm); (**c**) grinding depth—grinding wheel speed (v_w = 0.4 m/min).

4.3. Influence of Grinding Parameters on Burr Change in the Grind-Hardening Process

The burr appeared in three general patterns at different locations on the workpiece, as shown in Figure 9. The first is the Type I burr, as shown in Figure 9a. The radius of its burr root circle is large, the thickness, height, and cross-sectional area of the burr root are generally small, and the tip of the burr has almost no curl or a minimal degree of curl, which is mainly found at the cut-in or cut-out end of the workpiece. The second is the Type II burr, as shown in Figure 9b. Compared to the Type I burr, the Type II burr has a slightly larger root thickness and height, a smaller radius of the root circle, and a slightly curly tail of the burr, with a degree of curling less than 180°. The Type III burr is shown in Figure 9c. The root thickness and height of this burr is almost the same as that of the Type II burr, but the radius of the root circle is significantly smaller. The tail of the burr is curled seriously, with the degree of curling greater than or equal to 180°, and even turned over to the inside of the root circle. Type II burrs and Type III burrs were mainly distributed on both sides of the workpiece in the grinding stabilization zone. There were more Type II burrs at a smaller grinding depth or a larger feed speed; more Type III burrs occurred at a larger grinding depth, appearing on both sides near the cut-out zone.

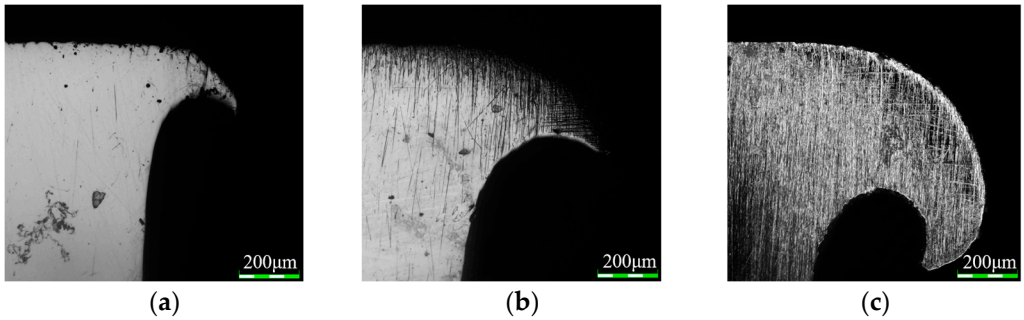

Figure 9. Basic morphology of burr on both sides (**a**) Type I burr (**b**) Type II burr, (**c**) Type III burr.

According to the previous study, the size of the burr on both sides has the greatest influence on the size and accuracy of the workpiece [14]. Therefore, this paper took the burr in both directions as the main research object to investigate the formation mechanism and variation pattern of burr size in the grind-hardening process. In the deburring process, the size of the burr cross-section directly affected the cost and efficiency of deburring. On this basis, this study proposed the burr cross-sectional area (S) as a parameter for assessing the quality of the prongs (burrs). It can be seen from Figure 10, with increasing grinding depth and decreasing workpiece feed speed, the burr cross-sectional area shows an increasing trend. With increasing grinding wheel speed, the burr cross-sectional area shows a trend of first increasing and then decreasing.

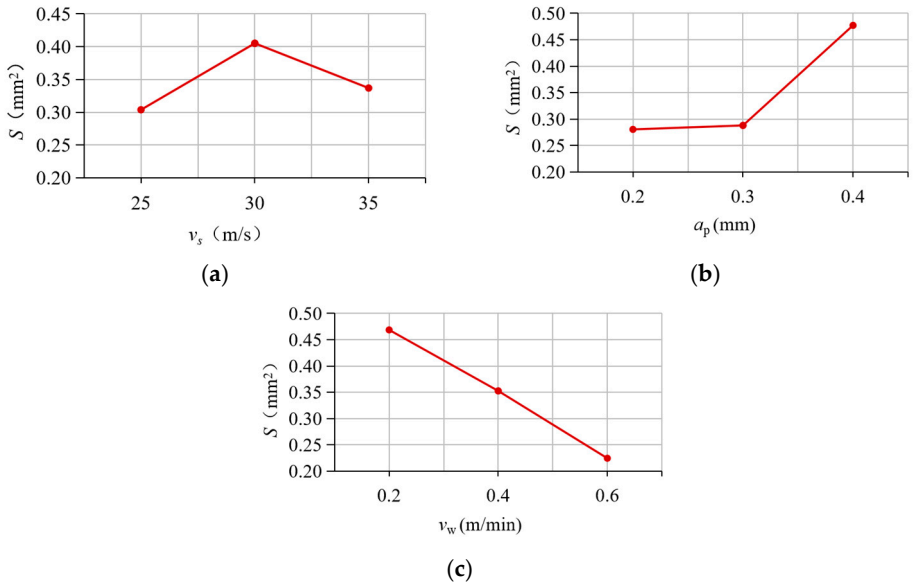

Figure 10. The influence of grinding dosage on the cross-section area of burrs on both sides: (**a**) grinding wheel speed, (**b**) grinding depth, and (**c**) the workpiece feed rate.

5. Multi-Response Optimization Analysis of Grinding Parameters Multi-Objective Response Optimization

5.1. Multi-Objective Response Optimization

The response surface method is a comprehensive optimization method developed on the basis of optimization theory and modern mathematical and statistical methods. It was proposed by Box and Wilson in 1951 [23]. Multiple response variables are often involved in product or process development. In this case, determining the optimal conditions for the input variables requires consideration of all responses, which is called a multi-response problem [24]. In 1980, Derringer and Suich first used the expectation function method for the optimization analysis of multiple responses [25].

The expectation function method is based on different types of objectives, such as large-the-better, small-the-better, or nominal-the-best, while simultaneously considering trade-offs among multiple optimization objectives [26,27]. The problem of optimizing the response variable Y can be reformulated as the maximization of a single desirability (d), which represents the satisfaction level and ranges from 0 to 1, with a value closer to 1 indicating higher satisfaction. When the estimated value of a response change y is $\hat{y}$, and the weight is r/t, variation can be reflected by the curve in Figure 11.

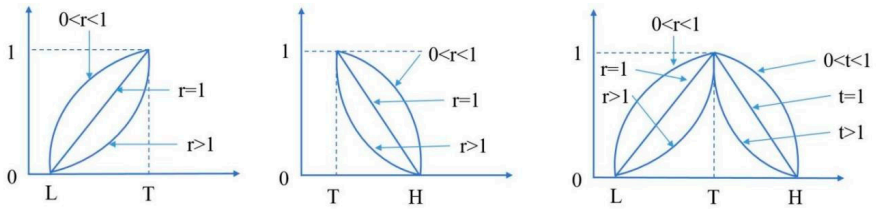

Figure 11. Expectation function diagram: (**a**) large-the-better, (**b**) small-the-better, and (**c**) nominal-the-best.

For the same problem, if the values of the lower bound, objective, and upper bound are set differently, the satisfaction degree may be different, but the final optimal solution is not affected [28]. The value of "Weight" ranges from 0.1 to 10, and the default value is $r = 1$. In this case, the target and the upper and lower limits are considered equally important. Reducing the emphasis on the goal sets r to a value less than 1. For greater emphasis on the goal, set a value greater than 1.

For multiple response variables, their optimization can be considered simultaneously. w_i is used to represent the "importance" of the ith response variable, and the desirability d_i of multiple response variables is combined into a composite agreement degree D, which is defined as:

$$D = \left(d_1^{w_1} d_1^{w_2} \ldots d_{\mathrm{k}}^{w_k}\right)^{\frac{1}{w}} = \left(\prod d_i^{w_i}\right)^{\frac{1}{w}} \quad (1)$$

where $W = \Sigma w_i$, which is the sum of all importance. At this point, D corresponds to the geometric mean of the individual d_i weighted by w_i. In particular, if these weights are all equal, the above equation can be simplified to a simple geometric mean of these degrees of agreement d_i:

$$D = (d_1 d_2 \ldots d_k)^k \quad (2)$$

In this paper, multi-objective optimization of grinding process parameters is performed regarding surface integrity in grind-hardening. After testing under the experimental conditions, the surface hardness of the hardened layer achieved the desired results, and no significant regular changes were observed. Therefore, it was not further optimized in this study. Multi-response optimization analysis of grind-hardening was carried out in Design-Expert 12 software, and the flow chart is shown in Figure 12.

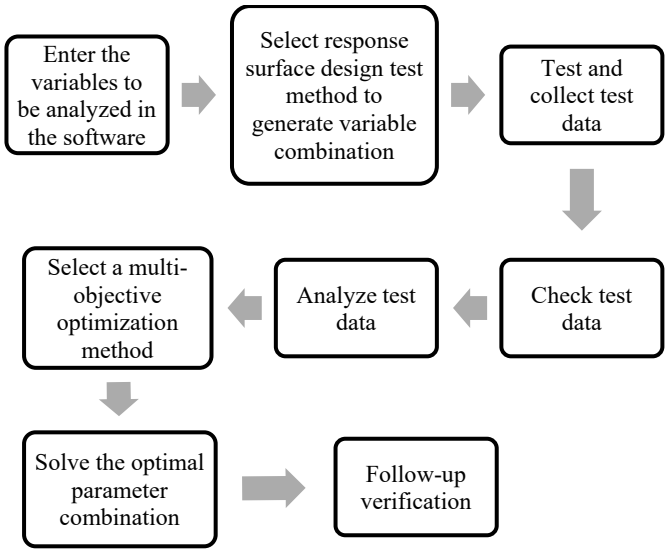

Figure 12. Flow chat of multi-objective optimization of response surface methodology.

As shown in Table 6, in different mechanical devices, different optimization criteria can be adopted for reasonable optimization of grind-hardening process parameters due to different application occasions and performance requirements for components.

Table 6. Optimization criteria for grind-hardened surface integrity of 42CrMo steel.

No.	Optimization Principle	Surface Integrity Index	Surface Quality Requirement	Applicable Component
Optimization criterion 1	Maximizing the hardened layer depth as the primary optimization factor.	Surface hardness and effective hardened layer depth, as well as favorable stress distribution, can effectively improve surface wear resistance.	Subject to severe alternating and shock loads, good wear resistance and fatigue strength are required [29,30].	Crankshafts and crankshaft connecting rods of automobile engines, large bearing rings for high-speed railways and wind power generation, etc.
Optimization criterion 2	Surface roughness as the primary optimization factor, and depth of the effective hardened layer as the secondary factor.	A smaller surface roughness and surface microhardness lead to a greater corrosion resistance.	The harsh working environment is easy to cause the corrosion and failure of components, resulting in higher requirements for the surface quality and surface corrosion resistance of components [31,32].	Marine equipment components, drilling joints, pump components, salvage equipment, and oil and gas drilling tools.
Optimization criterion 3	Effective hardened layer depth as the primary optimization factor, and surface roughness as the secondary factor.	The increased depth of the effective hardened layer and the presence of residual compressive stress in the surface layer of the specimen improve the rolling contact fatigue properties of the material.	In the case of heavy load for a long time, the more common failure form is fatigue damage, which requires the spindle bearing ring raceway to have a certain depth of hardened layer, thereby enhancing the fatigue strength [33,34].	Heavy duty bearings, large wind turbine spindle bearings.
Optimization criterion 4	The depth of the effective hardened layer is the main optimization factor, followed by surface roughness and edge quality.	Ensure the depth of the effective hardened layer while controlling surface roughness and edge quality.	Ensure machining accuracy; achieve a certain surface hardness to avoid surface quenching cracks [35,36].	Large-size, high-strength bolts for diesel engines, wind power generation equipment, and important components for ring cranes, etc.

Based on the four optimization criteria, different weights were set for surface roughness, depth of hardened layer, and burr cross-sectional area, as shown in Table 7. The "Weight" of the three parameters ranges from 0.1 to 10, and the importance ranges from "+" to "+++++". The maximum and minimum values of the three parameters were the experimental results of this study.

Table 7. Four optimization criteria.

Name		Goal	Lower Limit	Upper Limit	Lower Weight	Upper Weight	Importance
v_w (m/min)		Is in range	0.2	0.6	1	1	3
a_p (mm)		Is in range	0.2	0.4	1	1	3
v_s (m/s)		Is in range	25	35	1	1	3
Optimization criterion 1	*Ra* (μm)	Minimize	1.28	2.54	0.1	0.1	+
	S (mm^2)	Is target = 0.1470	0.1470	0.7112	0.1	0.1	+
	h (mm)	Maximize	1.16	2.64	10	10	+++++
Optimization criterion 2	*Ra* (μm)	Minimize	1.28	2.54	5	5	+++++
	S (mm^2)	Is target = 0.1470	0.1470	0.7112	0.1	0.1	+
	h (mm)	Is target = 2.64	1.16	2.64	1	1	++
Optimization criterion 3	*Ra* (μm)	Minimize	1.28	2.54	2	2	++
	S (mm^2)	Is target = 0.1470	0.1470	0.7112	0.1	0.1	+
	h (mm)	Maximize	1.16	2.64	5	5	++++
Optimization criterion 4	*Ra* (μm)	Minimize	1.28	2.54	1	1	+++
	S (mm^2)	Minimize	0.1470	0.7112	1	1	+++
	h (mm)	Maximize	1.16	2.64	1	1	++++

5.2. Analysis of Optimization Results

The optimal grinding parameter combination is shown in Table 8.

Table 8. The optimal results of each optimization criterion.

NO.	v_w (m/min)	a_p (mm)	v_s (m/s)	Ra (μm)	S (mm^2)	h (mm)	Desirability
Optimization criterion 1	0.200	0.400	33.995	2.000	0.681	2.635	0.925
Optimization criterion 2	0.200	0.200	32.322	1.355	0.345	1.988	0.711
Optimization criterion 3	0.200	0.400	32.368	1.942	0.698	2.630	0.607
Optimization criterion 4	0.200	0.214	34.375	1.473	0.325	2.049	0.693

(1) In optimization criterion 1, increasing the depth of the effective hardened layer was regarded as the primary optimization factor, and the specific parameter settings are shown in Table 7. As can be seen from Figure 13, with effective hardened layer depth as the main optimization response value, grinding depth and grinding linear speed have a significant impact on the degree of agreement, and grinding depth has the greatest impact. As the grinding depth and grinding wheel speed increase, the optimization desirability shows a significant upward trend. As can be seen from Table 8 and Figure 14 (optimization criterion 1), at the workpiece feed rate v_w = 0.2 m/min, grinding depth a_p = 0.4 mm, and grinding wheel speed v_s = 33.995 m/s, the surface roughness is Ra = 2.000 μm, the burr cross-sectional area is S = 0.681 mm^2, and the depth of the effective hardened layer is h = 2.635 mm. As a result, the overall optimization desirability of 0.925 can be achieved, thus realizing the desirable surface integrity.

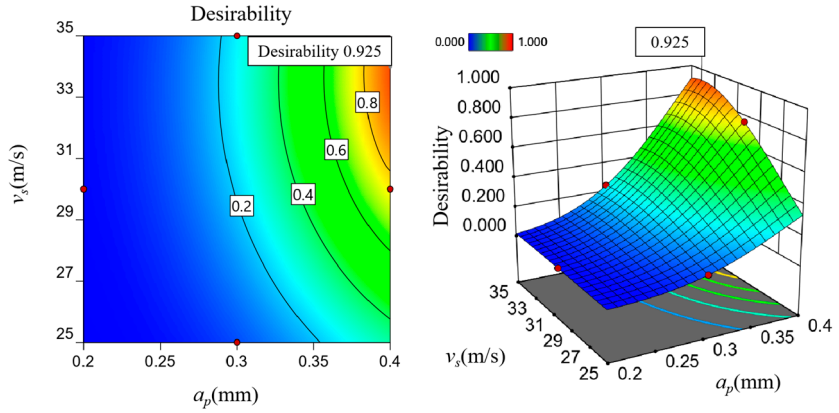

(**a**) (**b**)

Figure 13. Interactive effects of grinding linear speed and grinding depth on optimization desirability (v_w = 0.2 m/min). (**a**) contour diagram; and (**b**) response surface.

(2) In optimization criterion 2, surface roughness was regarded as the primary optimization factor, and the depth of the effective hardened layer was considered as the secondary factor. The specific parameter settings are shown in Table 7. As can be seen from Figure 15, as the workpiece feed rate decreases, the optimization desirability significantly increases. As the grinding wheel speed increases, the optimization desirability first increases and then decreases. As shown in Figure 16 and Table 7 (optimization criterion 2), at workpiece feed rate v_w = 0.2 m/min, grinding depth a_p = 0.2 mm, and grinding wheel speed v_s = 32.322 m/s, the surface roughness is Ra = 1.355 μm, the burr cross-sectional area is S = 0.345 mm^2, and the effective hardened layer depth is h = 1.988 mm. Under this condition, the overall optimization desirability of 0.711 can be achieved, thus realizing favorable surface integrity.

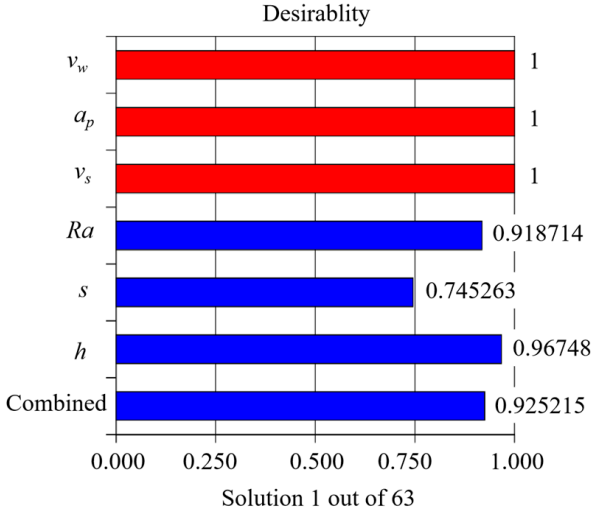

Figure 14. Desirability bar charts under optimization criterion 1.

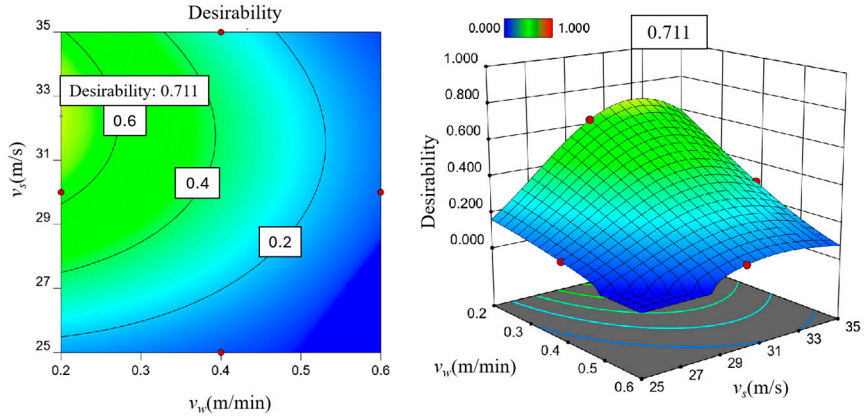

Figure 15. Interactive effects of workpiece feed speed and grinding wheel speed on optimization desirability (a_p = 0.2 mm). (**a**) contour diagram; and (**b**) response surface.

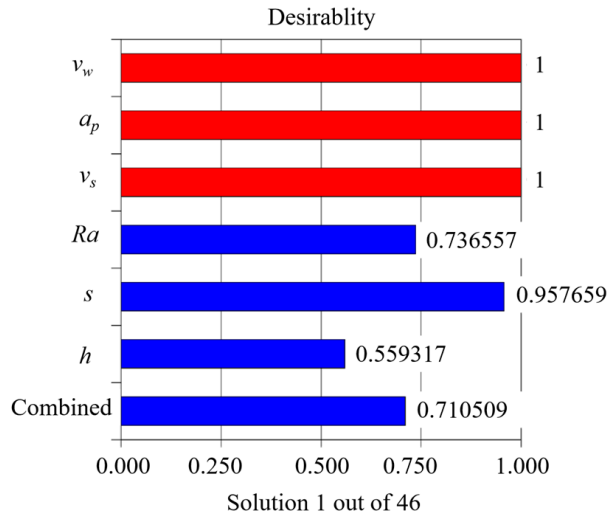

Figure 16. Desirability bar charts for optimization criterion 2.

(3) In the optimization criterion 3, the depth of the effective hardened layer was regarded as the primary factor, and surface roughness was considered as the secondary factor. The specific parameter settings are shown in Table 7. It can be seen from Figure 17 that the grinding depth and grinding wheel speed have a more significant effect on the optimization desirability. With increasing grinding depth, the optimization desirability tends to increase; with increasing grinding wheel speed, the optimization desirability tends to increase first and then decrease. As can be seen from Table 8 and Figure 18 (optimization criterion 3), at the workpiece feed rate v_w = 0.2 m/min, the grinding depth a_p = 0.4 mm, and the grinding wheel speed v_s = 32.368 m/s, the depth of hardened layer depth is h = 2.630 mm, the surface roughness is Ra = 1.942 μm, and the cross-sectional area of a burr is S = 0.698 mm^2. Under this condition, a favorable surface integrity can be realized at an overall optimization desirability of 0.607.

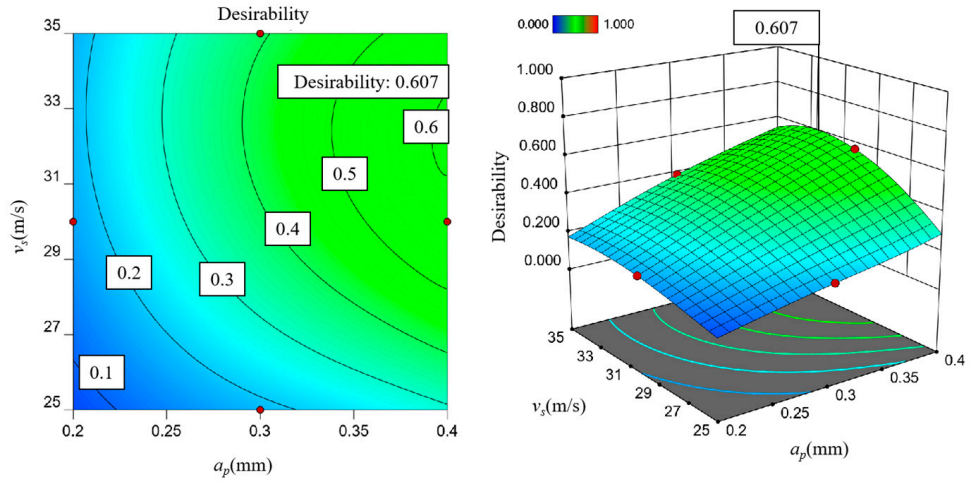

Figure 17. Interactive effects of grinding depth and grinding linear speed on optimization degree of agreement (v_w = 0.2 m/min). (**a**) contour diagram; and (**b**) response surface.

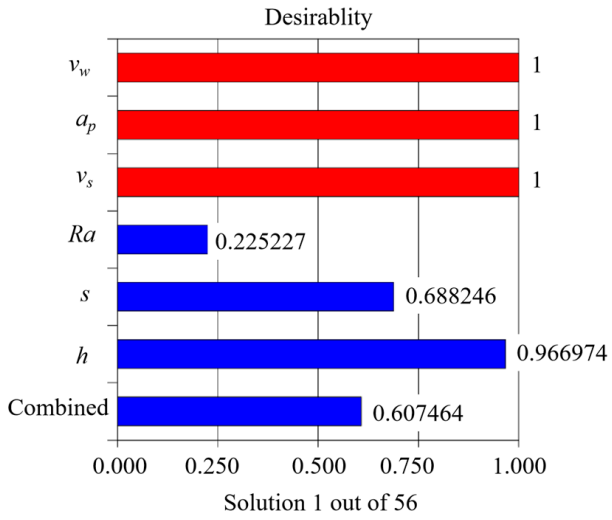

Figure 18. Bar chart of desirability under the optimization criterion 3.

(4) In optimization criterion 4, the depth of the effective hardened layer was taken as the primary factor, and surface roughness and edge quality were taken as the secondary factors. The specific parameter settings are listed in Table 7. It can be seen from Figure 19 that the effect of the grinding parameter on the overall optimization desirability is not very significant under optimization criterion 4. This is because a larger depth of the effective

hardened layer leads to greater surface roughness and the burr cross-sectional area, which cannot be effectively balanced. As shown in Table 8 and Figure 20 (optimization criterion 4), at the workpiece feed rate v_w = 0.2 m/min, the grinding depth a_p = 0.214 mm, and the grinding wheel speed v_s = 34.375 m/s, the depth of the effective hardened layer is h = 2.049 mm, the surface roughness is Ra = 1.473 μm, and the burr cross-sectional area is S = 0.325 mm^2. Therefore, a favorable surface integrity can be realized at an overall optimization desirability of 0.693.

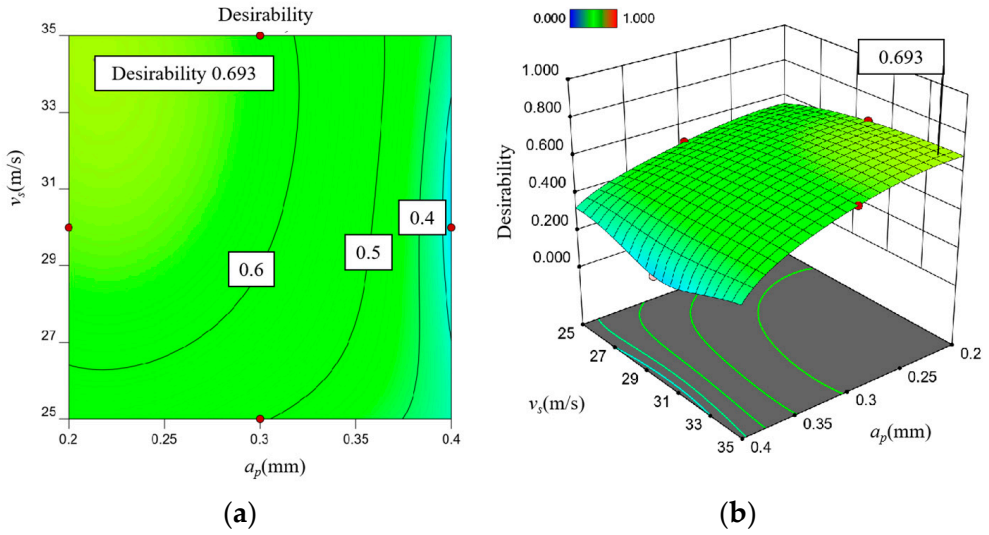

Figure 19. Interactive effects of grinding depth and grinding linear speed on optimization degree of agreement (v_w = 0.2 m/min). (**a**) contour diagram; and (**b**) response surface.

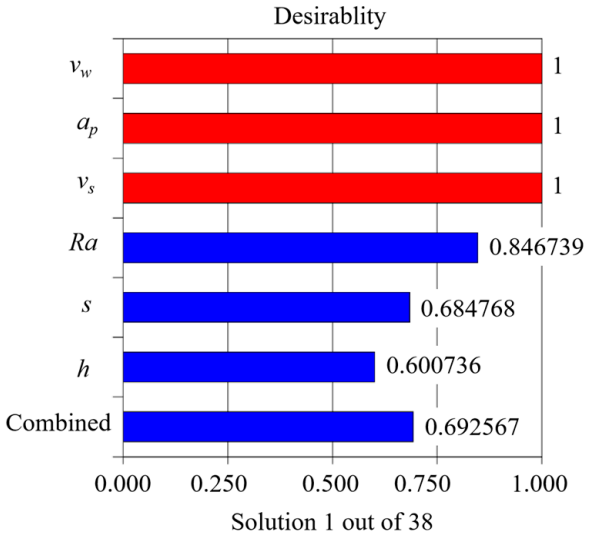

Figure 20. Bar chart of desirability under the optimization criterion 4.

5.3. Validation of the Optimization Model

Experimental validation was carried out based on the optimization results under the four criteria, as shown in Table 9.

Table 9. Validation results of the optimization model.

NO.	v_w (m/min)	a_p (mm)	v_s (m/s)		Ra (μm)	S (mm^2)	h (mm)
Optimization criterion 1	0.2	0.4	33.995	Measured value	2.56	0.6981	2.65
				Predicted value	2.000	0.681	2.635
				Relative error	$\lvert Ra'-Ra \rvert / Ra$ 21.86%	$\lvert S'-S \rvert / S$ 2.40%	$\lvert h'-h \rvert / h$ 0.56%
Optimization criterion 2	0.2	0.2	32.322	Measured value	1.51	0.3589	1.94
				Predicted value	1.355	0.345	1.988
				Relative error	$\lvert Ra'-Ra \rvert / Ra$ 10.28%	$\lvert S'-S \rvert / S$ 3.83%	$\lvert h'-h \rvert / h$ 2.46%
Optimization criterion 3	0.2	0.4	32.368	Measured value	2.37	0.6845	2.58
				Predicted value	1.942	0.698	2.630
				Relative error	$\lvert Ra'-Ra \rvert / Ra$ 18.06%	$\lvert S'-S \rvert / S$ 1.94%	$\lvert h'-h \rvert / h$ 1.94%
Optimization criterion 4	0.2	0.214	34.375	Measured value	1.90	0.3417	2.17
				Predicted value	1.473	0.325	2.049
				Relative error	$\lvert Ra'-Ra \rvert / Ra$ 22.47%	$\lvert S'-S \rvert / S$ 4.90%	$\lvert h'-h \rvert / h$ 5.58%

It can be seen from Table 9 that under the four optimization criteria, the prediction error for roughness is slightly larger (22.47%), which is consistent with the conclusion that surface roughness is not very suitable for constructing a prediction model using response surfaces. In the previous literature [16], other methods were applied to predict the surface roughness, and the prediction results had an error of less than 10% compared to the experimental results. Table 8 shows that the errors of the measured and optimized predicted values of the effective hardened layer depth and burr cross-sectional area were less than 6% in the four optimization criteria, and the prediction results were better. Although the proposed optimization model exhibits limitations in predicting surface roughness, it can offer valuable insights for evaluating surface integrity following grind-hardening from an engineering perspective.

6. Conclusions

Based on the results of the grind-hardening experiments, as well as the analysis of the optimization process and results obtained under four different optimization criteria for surface integrity evaluation, this paper draws the following conclusions:

The grinding depth has the greatest influence on the depth of the effective hardened layer and surface roughness. As the grinding depth increases, the depth of the effective hardened layer increases, leading to an increase in surface roughness and burr cross-sectional area and a decrease in the surface quality and edge quality. As the feed rate of the workpiece decreases, the depth of the effective hardened layer gradually increases, leading to increased surface roughness and decreased burr cross-sectional area. It can be seen that the influence of grinding parameters on surface quality, surface layer quality, and edge quality is inconsistent. Among the four optimization criteria, optimization criterion 1 with the depth of the effective hardened layer as the primary factor has the highest overall desirability of 0.925. In contrast, optimization criterion 3 with the depth of the effective hardened layer as the primary factor and surface roughness as the secondary factor has the lowest overall desirability of 0.607, exhibiting a large difference between the two optimization criteria. The experimental results of the optimization scheme showed that the surface roughness error predicted by this optimization method was large, but the prediction error of effective hardened layer depth and burr cross-sectional area were both lower than 6%, which can obtain a better result. Under the corresponding optimization criteria, the appropriate grinding parameters should be selected according to the actual engineering requirements, thus improving the surface integrity of the grind-hardening process.

Author Contributions: Conceptualization, G.W., C.S. and C.W.; methodology, C.W. and C.S.; software, C.W. and X.D.; validation, C.S. and C.W.; formal analysis, C.W.; investigation, C.W.; resources, C.W.; data curation, C.W. and X.D.; writing—original draft preparation, C.W.; writing—review and editing, G.W. and C.S.; visualization, C.W. and C.S.; supervision, G.W.; project administration, G.W.; funding acquisition, G.W. All authors have read and agreed to the published version of the manuscript.

Funding: This research was funded by the National Natural Science Foundation of China (NO. 50275066), and the National Major Science and Technology Project (NO. 2013ZX04009-030).

Institutional Review Board Statement: Not applicable.

Informed Consent Statement: Not applicable.

Data Availability Statement: Data is contained within the article.

Conflicts of Interest: The authors declare no conflicts of interest.

References

1. Brinksmeier, E.; Brockhoff, T. Randschicht-Wärmebehandlung dursh Schleifen. *Häerterei—Tech. Mitteilungen* **1994**, *49*, 327–330.
2. Brockhoff, T. Grinding-hardening: A comprehensive view. *Ann. CIRP* **1999**, *48*, 255–260. [CrossRef]
3. Wang, G.C.; Liu, J.D.; Pei, H.J.; Jia, Z.H.; Ma, L.J. Study on Forming Mechanism of Surface Hardening in Two-Pass Grinding 40Cr Steel. *Key Eng. Mater.* **2006**, *304–305*, 588–592. [CrossRef]
4. Liu, J.D.; Wang, G.C.; Wang, Z.; Fan, S.T. Experimental research of grind-hardening of 65Mn steel. *Mater. Sci. Forum* **2006**, *505–507*, 787–792. [CrossRef]
5. Liu, J.D.; Wang, G.C.; Wang, B.; Chen, K.M. Study on the Formation of Grind-Hardening of Steel AISI 1066. *Key Eng. Mater.* **2007**, *329*, 57–62. [CrossRef]
6. Nguyen, T.; Zhang, L.C.; Sun, D.L. Heat transfer in grinding-hardening of a cylindrical component. *Adv. Mater. Res.* **2011**, *325*, 35. [CrossRef]
7. Nguyen, T.; Zhang, L.C. Realisation of grinding-hardening in workpieces of curved surfaces—Part 1: Plunge cylindrical grinding. *Int. J. Mach. Tools Manuf.* **2011**, *51*, 309–319. [CrossRef]
8. Nguyen, T.; Liu, M.; Zhang, L.C.; Wu, Q.; Sun, D. An investigation of the grinding-hardening induced by traverse cylindrical grinding. *J. Manuf. Sci. Eng. Trans. ASME* **2014**, *136*, 051008. [CrossRef]
9. Liu, W.; Yuan, H.C.; Shi, X.Y.; Liu, T.; Du, S.S. Experimental study on residual stress in high-speed grinding of noncircular equidistant profle. *Int. J. Adv. Manuf. Technol.* **2022**, *123*, 3399–3406. [CrossRef]
10. Khodaii, J.; Adibi, H.; Barazandeh, F.; Rezaei, M.; Sarhan, A.A. Investigation of the surface integrity, flexural strength on the grinding of alumina for biomedical applications. *Precis. Eng.* **2021**, *67*, 110–122. [CrossRef]
11. Xiao, G.J.; Chen, B.Q.; Li, S.C.; Zhuo, X.Q.; Zhao, Z.Y. Surface integrity and fatigue performance of GH4169 superalloy using abrasive belt grinding. *Eng. Fail. Anal.* **2022**, *142*, 106764. [CrossRef]
12. Zhao, L.S.; Zhang, J.J.; Du, J.; Li, B.X.; Zhang, J.M.; Su, Z.S. Investigation on Surface Integrity of Nodular Cast Iron QT700-2 in Shape Adaptive Grinding. *Micromachines* **2023**, *14*, 276. [CrossRef] [PubMed]
13. Zou, J.F.; Pei, H.J.; Hua, C.L.; Jiao, B.; Wang, G.C. Residual stress distribution at grind-hardening layer surface of the 40Cr workpiece. *Mater. Res. Innov.* **2015**, *19*, 580–584. [CrossRef]
14. Jiao, B. Surface Integrity and Experimental Research on Grind-Hardening Process of 42CrMo Steel. Master's Thesis, Jiangsu University, Zhenjiang, China, 2016.
15. Guo, Y.; Xiu, S.C.; Liu, M.H.; Shi, X.L. Uniformity mechanism investigation of hardness penetration depth during grind-hardening process. *Int. J. Adv. Manuf. Technol.* **2017**, *89*, 2001–2010. [CrossRef]
16. Wang, C.Y.; Wang, G.C.; Shen, C.G. Analysis and prediction of grind-hardening surface roughness based on response surface methodology-BP neural network. *Appl. Sci.* **2022**, *12*, 12680. [CrossRef]
17. Hong, Y.; Sun, C.; Xiu, S.C.; Deng, Y.S.; Yao, Y.L.; Kong, X.N. Phase evolution and strengthening mechanism induced by grinding hardening. *Int. J. Adv. Manuf. Technol.* **2022**, *120*, 5605–5622. [CrossRef]
18. Zhao, X.F.; Liu, J.D.; Huang, S.W. Effect of grinding parameter on grinding-hardened case and its uniformity of nodular cast iron QT400. *Heat Treat. Met.* **2022**, *47*, 198–203.
19. Zhao, B.Q. *Heat Treatment Manual for Tool Steels*; China Machine Press: Beijing, China, 2014.
20. Cui, Z.Q.; Qin, Y.C. *Metallogy and Heat Treatment*; China Machine Press: Beijing, China, 2020.
21. *GB/T 33362-2016*; Conversion of Hardness Values of Metal Materials. Standardization Administration of China: Beijing, China, 2016.
22. Zhang, J. Experimental Study and Analysis of Single Plane Grind-hardening Process. Master's Thesis, Jiangsu University, Zhenjiang, China, 2018.
23. Box, G.E.P.; Wilson, K.B. On the experimental attainment of optimum conditions. *J. R. Stat. Soc.* **1951**, *13*, 1–45. [CrossRef]
24. Khuri, A. Multiresponse surface methodology. In *Handbook of Statistics: Design and Analysis of Experiments*; Ghosh, A., Rao, C.R., Eds.; Elsevier: Amsterdam, The Netherlands, 1996; Volume 13, pp. 377–406.

25. Derringer, G.; Suich, R. Simultaneous optimization of several response variables. *J. Qual. Technol.* **1980**, *12*, 214–219. [CrossRef]
26. Wang, J.J.; Ma, Y.Z.; Ouyang, L.H.; Tu, Y.L. Bayesian modeling and optimization for multi-response surfaces. *Comput. Ind. Eng.* **2020**, *142*, 106357. [CrossRef]
27. Jeong, I.J.; Kim, K.J. An interactive desirability function method to multiresponse optimization. *Eur. J. Oper. Res.* **2009**, *195*, 412–426. [CrossRef]
28. Zhang, Y.B.; Zhang, W.C.; Li, Y.S.; Zhao, L.M.; Li, H.Y.; Lei, Y.B.; Yang, Y.Q. Experimental of Consolidation Performance of Laterite in Plateau Based on RSM. *Mater. Rep.* **2023**, *37*, 259–264.
29. Wu, H.; Lin, S.Y.; Li, X.K.; Gong, Y.H.; Wei, D.Q. Effect of induction hardening on microstructure and properties of 42CrMo steel crankshaft connecting rod journal. *Jinshu Rechuli/Heat Treat. Met.* **2022**, *47*, 119.
30. Wei, S.T.; Wu, C.J.; Zheng, L.G.; Hu, X.Q.; Lu, S.P. Effect of surface quenching process on hardened layer of 42CrMosteel for large bearing ring. *Heat Treat. Met.* **2022**, *47*, 218–223.
31. Liu, J.C. Study on Surface Integrity and Corrosion Resistance of42CrMoSteel after Ultrasonic Surface Rolling Process. Master's Thesis, Dalian Maritime University, Dalian, China, 2022.
32. Zhao, Y.H.; Wang, K.; Wang, Z.L.; Shi, M.J.; Li, F.F.; Ye, C.C. Effect of different surface treatments of 42CrMo steel piston rod on its corrosion resistance in sodium chloride solution. *Int. J. Electrochem. Sci.* **2022**, *17*, 1452–3981. [CrossRef]
33. Zhang, Q.L.; Huang, H.; Tang, Z.H.; Li, G.C.; Niu, Q.A.; Chen, Z.J.; Du, Y.Q.; Yao, J.H. Rolling Wear and Fatigue Damage Behavior of Laser-Induction Hybrid Quenching on 42CrMo Steel. *Chin. J. Lasers* **2022**, *49*, 250–261.
34. Zhang, Q.L.; Tong, W.H.; Chen, Z.J.; Yao, J.H.; Li, Z.G.; Feng, K.; Kovalenko, V.S. Effect of Spot Size on Geometrical Characteristics of Laser Deep Quenching Hardened Layer of 42CrMo Steel. *Surf. Technol.* **2020**, *49*, 254–261.
35. Jiao, L.; Shang, H.K.; He, J.F.; Zhao, Y.J.; Zhang, W.M.; Li, W.M.; Zhou, L.M. Fracture failure analysis of 42CrMo steel high strength bolts for diesel engine. *Heat Treat. Met.* **2021**, *46*, 245–249.
36. Chen, J.D.; Mo, W.L.; Wang, P.; Lu, S.P. Effects of tempering temperature on the impact toughness of steel 42crmo. *Acta Metall. Sin.* **2012**, *48*, 1186–1193. [CrossRef]